

# EIT-based Vector Magnetometry in Linear Polarized Light

V. I. Yudin<sup>1,2,3</sup>, A. V. Taichenachev<sup>1,2</sup>, Y. I. Dudin<sup>4</sup>, V. L. Velichansky<sup>4,5</sup>, A. S. Zibrov<sup>6</sup>, S. A. Zibrov<sup>5</sup>

<sup>1</sup>*Laser Physics Institute, Siberian Division RAS, Novosibirsk, 630090, Russia*

<sup>2</sup>*Novosibirsk State University, Novosibirsk, 630090, Russia*

<sup>3</sup>*Novosibirsk State Technical University, Novosibirsk, 630092, Russia*

<sup>4</sup>*Moscow State Engineering and Physics Institute, Moscow, 115409, Russia*

<sup>5</sup>*Lebedev Physical Institute, RAS, Moscow, 117924, Russia*

<sup>6</sup>*Physics Department, Harvard University, Cambridge, MA, 02138, USA*

(Dated: April 15, 2019)

We develop a generalized principle of EIT vector magnetometry based on the high-contrast EIT-resonances and the symmetry of the atom-light interactions in the linear polarized bichromatic field. A realization of such vector magnetometer on  $D_1$  line of  $^{87}\text{Rb}$  has been demonstrated. The proposed compass-magnetometer has an increased immunity to the shifts produced by quadratic Zeeman and ac-Stark effects, atom-buffer gas and atom-atom collisions. In our proof-of-principle experiment the detected sensitivity of the magnetic field orientation is  $10^{-3}\text{deg/Hz}^{1/2}$ , which is limited by laser intensity fluctuations, the polarization quality and the magnetic field magnitude.

PACS numbers: 07.55.Ge, 32.30.Dx, 32.70.Jz

## I. INTRODUCTION

The pure quantum state is a basic concept of quantum physics, which plays a key role in various applications. They are magnetometry, frequency standards, laser cooling, quantum information science, nonlinear optics and also “slow” and “fast” light experiments. To all these applications the effect of electromagnetically induced transparency (EIT) [1–4] is successfully employed.

The idea of EIT scalar magnetometer was suggested in [5]. The steep dispersion of EIT media promises a dramatic improvement of the scalar magnetometer sensitivity. Since then different schemes of EIT magnetometers are considered. Among them are those based on nonlinear Faraday effect in manifold of one ground state [6–8] and the scheme in which the frequency shift of Zeeman sublevels of both ground states is detected [9]. The sensitivity of EIT magnetometers still is in the same range as the ones with optical pumping [10, 11]. However, a recent modification of optical pumping magnetometers, so-called SERF-magnetometers with suppressed spin-exchange broadening, drastically improves sensitivity by a factor of  $10^3$  and overcomes the sensitivity of SQUID magnetometers ( $10^{-15}\text{ T/Hz}^{1/2}$ ) [12]. Unfortunately, SERF-magnetometers work in small fields significantly less than geomagnetic ones,  $\leq 0.1\text{ }\mu\text{T}$ .

For many applications preferable to know not only scalar but vector distribution of the magnetic field as well. To achieve this additional coils are installed for each  $X$ ,  $Y$  and  $Z$  axes into the scalar magnetometer. A small modulation of the magnetic field along axes caused by coils gives the information about  $B_x$  and  $B_y$  field components [13–15], which allows to reconstruct the orientation of the vector  $\mathbf{B}$ . The reviews of existing all-optical magnetometers were published in [16, 17].

In the present paper we show that the employing of the unique features of high-contrast EIT resonances of the  $D_1$

line of  $^{87}\text{Rb}$  allows us to find new principles of the atomic vector magnetometry and implement a corresponding device, in which the scalar and vector properties can be used separately or integrated in one device.

## II. GENERAL DESCRIPTION OF THE TASK

EIT phenomenon is closely connected to the so-called coherent population trapping (CPT) [1, 2] for which the atom-field interaction  $-(\hat{\mathbf{d}}\mathbf{E})$  of the pure quantum state  $|dark\rangle$  is nullified:

$$-(\hat{\mathbf{d}}\mathbf{E})|dark\rangle = 0. \quad (1)$$

This state is a special coherent superposition of the ground state Zeeman sublevels, which neither absorbs nor emits light. Dark states lead to the highest contrast and transmission of EIT resonances. Thus, the way how to prepare the pure states is crucial for any of mentioned applications.

The generalized problem of the creation of the pure quantum states by bichromatic elliptically polarized field was solved in [18]. In [19–21] it was theoretically and experimentally demonstrated that  $D_1$  line of  $^{87}\text{Rb}$  has a unique level structure for the creation of pure dark states by the bichromatic linear polarized light (so-called lin||lin field), when the resonant interaction occurs via upper energy level  $F_e=1$ . There are two pairs of the dark states, where each dark state corresponds to the separated  $\Lambda$ -scheme (see Fig. 1). One pair ( $\Lambda_1$  and  $\Lambda_2$  schemes in Fig. 1a) is insensitive to the magnetic field (on the linear contribution) and produces the following two-photon transitions:  $|F_1=1, m=-1\rangle \leftrightarrow |F_2=2, m=+1\rangle$  and  $|F_1=1, m=+1\rangle \leftrightarrow |F_2=2, m=-1\rangle$ . The other one ( $\Lambda_3$  and  $\Lambda_4$  in Fig. 1b) is sensitive to the magnetic field with two-photon transitions:  $|F_2=2; m=-1\rangle \leftrightarrow |F_1=1; m=-1\rangle$  and  $|F_2=2; m=+1\rangle \leftrightarrow |F_1=1; m=+1\rangle$ .

In our experiments the EIT resonances of these pairs have a high contrast (50%) and transmission (60%) (see Fig. 2, solid line).

Note, the magnetically insensitive EIT resonance is a product of two overlapped  $\Lambda_1$  and  $\Lambda_2$  transitions and because of the high contrast and 1.33 times less quadratic dependence on the magnetic field compared to the regular atomic clock transition  $|F_1 = 1, m = 0\rangle \leftrightarrow |F_2 = 2, m = 0\rangle$  [22, 23] is a promising candidate for a atomic clock. Contrarily to  $\Lambda_{1,2}$ , the  $\Lambda_{3,4}$ -resonances are magneto-sensitive and can be used as a detector of the magnetic field's magnitude.

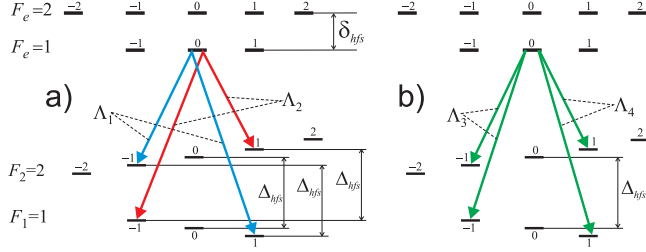


FIG. 1: Pure states of the  $D_1$  line of  $^{87}\text{Rb}$ : non-sensitive (a) and sensitive to magnetic field (b). Here we do not show Zeeman shifts for the upper hyper-fine levels with  $F_e=1,2$ .

Thus, in the present paper to create the quantum dark states (1) for  $D_1$  line of  $^{87}\text{Rb}$  we will use (in conformity with [20]) the linear polarized bichromatic running wave  $\mathbf{E}(\mathbf{r}, t)$  with near frequencies  $\omega_1$  и  $\omega_2$ , and with wavevector  $\mathbf{k}$  (i.e.  $\text{lin}||\text{lin}$  configuration):

$$\mathbf{E}(\mathbf{r}, t) = (E_1 e^{-i\omega_1 t} + E_2 e^{-i\omega_2 t}) e^{i\mathbf{k}\mathbf{r}} \mathbf{e} + c.c., \quad (2)$$

where  $\mathbf{e}$  is a unit vector of the linear polarization, and  $E_{1,2}$  are the scalar amplitudes of corresponding frequency components. The interaction occurs at the presence of the static magnetic field  $\mathbf{B}$ . If the  $z$ -axis is directed along vector  $\mathbf{B}$ , then the vector  $\mathbf{e}$  can be expressed in a spherical basis  $\{\mathbf{e}_0 = \mathbf{e}_z, \mathbf{e}_{\pm 1} = \mp(\mathbf{e}_x \pm i\mathbf{e}_y)/\sqrt{2}\}$  by the following form:

$$\mathbf{e} = \sum_{q=0,\pm 1} e^{(q)} \mathbf{e}_q = \cos \theta \mathbf{e}_0 - \frac{\sin \theta}{\sqrt{2}} (\mathbf{e}_{+1} - \mathbf{e}_{-1}), \quad (3)$$

where  $\theta$  is the angle between vectors  $\mathbf{B}$  and  $\mathbf{e}$ ;  $e^{(q)}$  are the contravariant components of the vector  $\mathbf{e}$ . Note that for the linear polarization its circular components ( $\sigma_{\pm}$ ) are always equal.

$$|e^{(+1)}| = |e^{(-1)}| = |\sin \theta|/\sqrt{2} \quad (4)$$

As it will be shown below, the symmetry of (4) is one of principal points of EIT magnetometry in the linear polarized field.

In the resonant approximation we assume that the frequency component  $\omega_j$  ( $j=1,2$ ) excites atoms only from the hyper-fine ground level  $F_j$  (see Fig. 1). Hereinafter we will use the interaction representation:

$$e^{-i\mathcal{E}_{F_m} t/\hbar} |F, m\rangle \rightarrow |F, m\rangle,$$

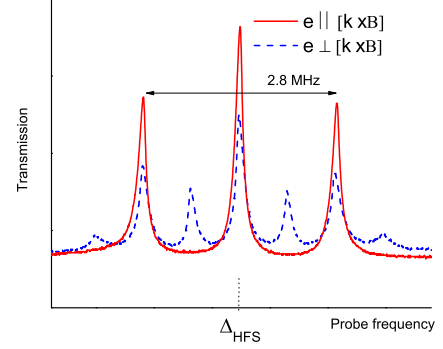


FIG. 2: Transmission of EIT resonances: (solid line) – the case  $\mathbf{e}||\mathbf{n}$ . The central resonance corresponds to the  $\Lambda_1$  and  $\Lambda_2$  schemes (see Fig. 1a). This resonance has 120 kHz width and  $\sim 60\%$  transmission. (dash line) – the case  $\mathbf{e}\perp\mathbf{n}$ . Magnetic field has magnitude 1 G, the angle between  $\mathbf{B}$  and  $\mathbf{k}$  equals  $20^\circ$ .

where  $\mathcal{E}_{F_m}$  is the energy of the level  $|F, m\rangle$  in which Zeeman shift is included. The operator of an atomic-field interaction  $-(\hat{\mathbf{d}}\mathbf{E}) = \hat{V} + \hat{V}^\dagger$  under resonant approximation takes the form:

$$\hat{V} = e^{i\mathbf{k}\mathbf{r}} \sum_{q=0,\pm 1} e^{(q)} \times \quad (5)$$

$$\left[ E_1 \sum_{F_e, \mu, m_1} d_{F_e F_1} e^{-i\delta_{\mu m_1}^{(1)} t} C_{F_1 m_1, 1q}^{F_e \mu} |F_e, \mu\rangle \langle F_1, m_1| + \right.$$

$$\left. E_2 \sum_{F_e, \mu, m_2} d_{F_e F_2} e^{-i\delta_{\mu m_2}^{(2)} t} C_{F_2 m_2, 1q}^{F_e \mu} |F_e, \mu\rangle \langle F_2, m_2| \right].$$

Here  $d_{F_e F_1}$  and  $d_{F_e F_2}$  denote a reduced matrix elements of corresponding optical transitions  $F_1 \rightarrow F_e$  and  $F_2 \rightarrow F_e$ ;  $C_{F_j m_j, 1q}^{F_e \mu}$  is Clebsch-Gordan coefficient; and  $\delta_{\mu m_j}^{(j)} = \omega_j - (\mathcal{E}_{F_e \mu} - \mathcal{E}_{F_j m_j})/\hbar$  (where  $j = 1, 2$ ) are corresponding one-photon detunings.

For alkali-earth atoms with nuclear spin  $S_n$  we have  $F_1 = (S_n - 1/2)$  and  $F_2 = (S_n + 1/2)$ . The corresponding electronic ground-state Landé factors have the same absolute value, but the opposite signs,  $g = -g_{F_1} = g_{F_2} = (S_n + 1/2)^{-1}$  (for  $^{87}\text{Rb}$   $g=1/2$ ). Then in the linear approximation on the magnetic field  $\mathbf{B}$  and in an absence of the nuclear magnetic momentum it is easy to count the number of splitted two-photon resonances. For arbitrary directed  $\mathbf{B}$  there are  $(4S_n + 1)$  two-photon resonances on Raman detuning  $\delta_R = (\omega_1 - \omega_2 - \Delta_{hfs})$  with centers in the points  $\delta_R = l g \mu_B |\mathbf{B}|/\hbar$  ( $l = -2S_n, \dots, 2S_n$ ), where  $\mu_B$  is Bohr magneton. For example, in  $^{87}\text{Rb}$  ( $S_n = 3/2$ ) we have seven two-photon resonances (see Fig. 2, blue dash line). In the particular case  $\mathbf{B} \perp \mathbf{e}$  the number of the two-photon resonances equals to  $2S_n$ , i.e. three resonances for  $^{87}\text{Rb}$  (see Fig. 2, red solid line).

### III. EIT-BASED 3D COMPASS

First of all we examine in details the central resonance (near  $\delta_R=0$ ), which is magnetically insensitive in the linear approximation of  $\mathbf{B}$ . It will be shown below that the exactly this resonance can be used as a base of the vector magnetometry due to a strong dependence of the transmission from the mutual orientation of vectors  $\mathbf{e}$  and  $\mathbf{B}$  (i.e. the angle  $\theta$  in Eq.(3)). It should be emphasized that for formation of the central two-photon resonance the following two transitions take place:  $|F_1, m=-1\rangle \leftrightarrow |F_2, m=+1\rangle$  and  $|F_1, m=+1\rangle \leftrightarrow |F_2, m=-1\rangle$ , for which the energy difference is equals  $\hbar\Delta_{hfs}$  (see Fig. 1a). The third two-photon transition  $|F_1, m=0\rangle \leftrightarrow |F_2, m=0\rangle$  (between magnetically insensitive sublevels) is strongly suppressed due to a destructive interference between contributions from the opposite circular components  $\sigma_{\pm}$ .

In case of the resolved upper hyper-fine structure (see  $F_e=1,2$  in the Fig. 1) the two-photon resonance can be excited via a particular level. Further we assume that frequency components (2) are at the resonance of the single hyper-fine level  $F_e=1$  (see Fig. 1). Now let us consider a special case, when the vectors  $\mathbf{e}$  and  $\mathbf{B}$  are mutually orthogonal ( $\theta=\pi/2$ ), and, therefore, in the decomposition (3) only two equal circular components occur:  $\mathbf{e} = -(\mathbf{e}_{+1} - \mathbf{e}_{-1})/\sqrt{2}$ . It is seen from Fig. 1a that there is a two-photon resonance of pure  $\Lambda_1$ -scheme with Zeeman sublevels  $|F_1=1, m=+1\rangle$  and  $|F_2=2, m=-1\rangle$ . Absolutely analogous  $\Lambda_2$ -scheme is realized with other sublevel pairs  $|F_1=1, m=-1\rangle$  and  $|F_2=2, m=+1\rangle$ . Both these  $\Lambda_{1,2}$ -schemes are formed via same common upper sublevel  $|F_e=1, m=0\rangle$ . As it was mentioned before, the frequency of these two-photon resonances equals (neglecting nuclear magneton) the frequency of the (0-0) resonance between sublevels  $|F_1=1, m=0\rangle$  and  $|F_2=2, m=0\rangle$ .

The uniqueness of the situation is, in fact, in the overlapping of two dark states  $|dark\rangle_{\Lambda_1}$  and  $|dark\rangle_{\Lambda_2}$ , which occur at exactly at two-photon resonance,  $\delta_R = 0$ . These states behave as describe the equation (1) and have the following forms:

$$|dark\rangle_{\Lambda_{1,2}} = \frac{\sqrt{3}E_2|F_1, m = \pm 1\rangle \mp E_1|F_2, m = \mp 1\rangle}{\sqrt{|E_1|^2 + 3|E_2|^2}}. \quad (6)$$

The presence of such dark states in the case  $\mathbf{e} \perp \mathbf{B}$  leads to a high contrast of the central dark resonance near  $(\omega_1 - \omega_2) = \Delta_{hfs}$  (i.e.  $\delta_R \approx 0$ ). This fact was predicted and experimentally demonstrated in [19, 20].

In the general case of  $\theta \neq \pi/2$  (that is  $\cos(\theta) \neq 0$ ) there are no pure  $\Lambda$ -schemes due to  $\pi$ -polarized (along  $\mathbf{B}$ ) component in decomposition (3). It leads to a smaller amplitude and contrast of the magnetically insensitive two-photon resonance in comparison to the case of  $\theta=\pi/2$ . It is precisely this fact that will be used as a base for determination of the magnetic field orientation (i.e. compass).

The basic idea of our method can be explained in the following way. Assume the wavevector  $\mathbf{k}$  and the vector  $\mathbf{B}$

have an arbitrary mutual orientation. As a measurand we will use the amplitude of the central resonance (absorption/transmission or fluorescence) (see Fig. 2). While making a full turn of vector  $\mathbf{e}$  around  $\mathbf{k}$  one can twice find the position when  $\mathbf{e}$  and  $\mathbf{B}$  are orthogonal to each other. To be certain, these situations arise if  $\mathbf{e} \parallel \mathbf{n}$ , where  $\mathbf{n} = [\mathbf{k} \times \mathbf{B}]$  (see Fig. 3). These cases correspond to dark states (6), which lead to the maximal amplitude and contrast of the central resonance (as it was explained above).

Consider the dependence of the dark resonance amplitude on the orientation of vector  $\mathbf{e}$  (at fixed  $\mathbf{k}$ ). This dependence can be presented as a function  $A_{\mathbf{k}}(\varphi)$ , where  $\varphi$  is an angle between vectors  $\mathbf{e}$  and  $\mathbf{n}$  (see Fig. 3). Even the qualitative analysis, provided above, leads to the conclusion that the function  $A_{\mathbf{k}}(\varphi)$  reaches its maximum at  $\varphi=0$ , i.e. when  $\mathbf{e} \perp \mathbf{B}$ .

The essence of the measuring procedure could be represented by the following algorithm. At first, for a chosen vector  $\mathbf{k}=\mathbf{k}_1$ , we register the  $A_{\mathbf{k}_1}(\varphi)$  dependency by rotating the polarization vector  $\mathbf{e}$ . The maximum of this dependency corresponds to the direction of the vector  $\mathbf{n}=[\mathbf{k}_1 \times \mathbf{B}]$ , which gives us the equation for the plane  $(\mathbf{k}_1, \mathbf{B})$ , formed by the vectors  $\mathbf{k}_1$  and  $\mathbf{B}$ . Repeating the same procedure for another orientation of the wavevector  $\mathbf{k}=\mathbf{k}_2$  (for example,  $\mathbf{k}_2 \perp \mathbf{k}_1$ ) we determine the equation for the plane  $(\mathbf{k}_2, \mathbf{B})$ . The intersection line of two planes  $(\mathbf{k}_1, \mathbf{B})$  and  $(\mathbf{k}_2, \mathbf{B})$  coincides with magnetic line of force, that determines the 3D orientation of the vector  $\mathbf{B}$  with uncertainty of the sign.

The basic principle of our method is quite universal and does not depend on different experimental parameters (such as the  $|E_1/E_2|$  ratio, one-photon detuning, relaxation constants, nuclear magnetic momentum, and so on). This can be seen from general symmetry of the task. Indeed, let us have an arbitrary polychromatic wave, which is propagating along a single direction  $\mathbf{k}$ , and all frequency components have the same linear polarization  $\mathbf{e}$ . Also we assume that the atomic medium is isotropic in the absence of the light field. By the signal  $S(\mathbf{e}, \mathbf{B})$  we will understand an arbitrary scalar value which depends on the mutual orientation of the vector  $\mathbf{e}$  and  $\mathbf{B}$ . In sense of this definition  $S(\mathbf{e}, \mathbf{B})$  could be full transmission (or absorption) or fluorescence signal. The analysis of Bloch equations leads to the following generalized relationship:

$$S(\mathbf{e}, \mathbf{B}) = S(-\mathbf{e}, \mathbf{B}) = S(\mathbf{e}, -\mathbf{B}). \quad (7)$$

This relationship comes from a symmetry of Clebsch-Gordan coefficients  $|C_{Fm,1q}^{F'm'}| = |C_{F-m,1-q}^{F'-m'}|$ , and the equality of circular components (4) in arbitrary coordinate system.

Consider the configuration represented in Fig. 3, where the light field has polarization  $\mathbf{e}(\varphi)$ . Let us perform a mathematical reflection in relation to the plane  $(\mathbf{k}, \mathbf{B})$ . This leads to the substitution of the polarization vector  $\mathbf{e}(\varphi)$  by  $(-\mathbf{e}(-\varphi))$ , but for the *pseudovector* of the magnetic field it leads to  $\mathbf{B} \rightarrow (-\mathbf{B})$ . It is known, that the

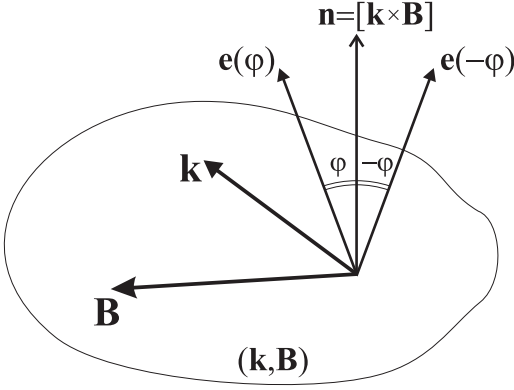


FIG. 3: Orientation of the magnetic field  $\mathbf{B}$ , wavevector  $\mathbf{k}$  and polarization  $\mathbf{e}$  of the optical field.

mathematical reflection does not affect a scalar signal, i.e. the following relationship is obtained:

$$S(\mathbf{e}(\varphi), \mathbf{B}) = S(-\mathbf{e}(-\varphi), -\mathbf{B}). \quad (8)$$

By combining (7) and (8) we finally achieve

$$S(\mathbf{e}(\varphi), \mathbf{B}) = S(\mathbf{e}(-\varphi), \mathbf{B}), \quad (9)$$

i.e. the scalar signal is an even function of the angle  $\varphi$ . It signifies that the point  $\varphi=0$  (i.e.  $\mathbf{e} \perp \mathbf{B}$ ) corresponds to the local extremum (maximum or minimum) of the  $S(\mathbf{e}(\varphi), \mathbf{B})$  dependence, which is obtained by rotating the polarization vector  $\mathbf{e}$  around wavevector  $\mathbf{k}$ .

Here we should make a comment, that the described principle of the vector magnetometry is valid for arbitrary atoms, lines ( $D_1$  or  $D_2$ ) and an arbitrary spectrum of the linear polarized light (including monochromatic light). However, the use of the dependence  $A(\varphi)$  for central resonance excited by the bichromatic field at the  $^{87}\text{Rb}$   $D_1$  line is the best choice for the demonstration of the compass principle, because of the significant signal/noise ration and transmission.

#### IV. EIT DIFFERENTIAL MAGNETOMETER

As it was shown above, rotating the linear polarization  $\mathbf{e}$  around the wavevector  $\mathbf{k}$  and analyzing the corresponding dependence of amplitude  $A(\varphi)$  of the central (magnetically insensitive) dark resonance we always can find the condition  $\mathbf{e} \perp \mathbf{B}$ . In this section we will consider two end magnetically sensitive resonances (see Fig. 2, red solid line), which are connected with  $\Lambda_{3,4}$ -systems at the Fig. 1b (i.e. with two-photon transitions  $(-1) \leftrightarrow (-1)$  and  $(+1) \leftrightarrow (+1)$ ). In the case of  $\mathbf{e} \perp \mathbf{B}$  the amplitudes of these resonances become also maximal, because at the exact two-photon resonance (i.e.  $\delta_R = \pm 2g\mu_B|\mathbf{B}|/\hbar$ ) there are the following two dark states:

$$|dark\rangle_{\Lambda_{3,4}} = \frac{\sqrt{3}E_2|F_1, m = \mp 1\rangle \pm E_1|F_2, m = \mp 1\rangle}{\sqrt{|E_1|^2 + 3|E_2|^2}}. \quad (10)$$

Measuring the distance between these end resonances  $\Delta_{\pm}$  we find the value  $|\mathbf{B}|$ . In the linear approximation (on  $|\mathbf{B}|$ ) we apply the formula  $|\Delta_{\pm}| = \gamma'|\mathbf{B}|$ , where  $\gamma' = 2(g_{F_2} - g_{F_1})\mu_B/\hbar$  is an effective gyromagnetic ratio. Subject to the nuclear magneton for  $^{87}\text{Rb}$  [24, 25] we should use the following values for  $g$ -factors:  $g_{F_1} = -0.501827$  and  $g_{F_2} = 0.499836$ . Thus, in our case  $\gamma' = 2.803905 \times 10^{10}$  Hz/T.

Taking into account a symmetry of the atom-light interactions in the linear polarization one can predict some important properties for such magnetometry. Indeed, this frequency-differential magnetometer is immune to:

- (I) the collisional shift arising due to the interaction with an isotropic buffer gas.
- (II) the quadratic Zeeman shift of magnetic sublevels.
- (III) the shift arising due to the atom-atom interaction (including spin-exchange) between working atoms (here between  $^{87}\text{Rb}$  atoms).
- (IV) and has the significant suppression of the ac-Stark shift.

The property (I) is a result of the equality of the collisional shifts of any Zeeman sublevels  $|F, m\rangle$  (for given  $F$ ) in an isotropic buffer gas. Property (II) is also quite obvious considering that even power terms of Zeeman shift of the  $m \leftrightarrow m$  and  $-m \leftrightarrow -m$  transitions make contribution with opposite signs. This feature is valid for any atom (i.e. not only  $^{87}\text{Rb}$ ) and line ( $D_1$  or  $D_2$ ).

The property (III) is a result of an interaction of atoms with linear polarized light. Indeed, let us consider the atomic density matrix  $\hat{\rho}$ , which describes the distribution among Zeeman sublevels:

$$\hat{\rho} = \sum_{F', m', F'', m''} \rho_{m'm''}^{F'F''} |F', m'\rangle \langle F'', m''|, \quad (11)$$

where  $\rho_{m'm''}^{F'F''}$  are matrix elements. We designate the atomic distribution for two-photon resonances  $(+1) \leftrightarrow (+1)$  and  $(-1) \leftrightarrow (-1)$  as  $\rho_{m'm''}^{(+F'F'')}$  and  $\rho_{m'm''}^{(-F'F'')}$  respectively. From the symmetry of the problem and neglecting some insignificant details (for example a small variation of the one-photon detuning) it follows that  $|\rho_{m'm''}^{(+F'F'')}| = |\rho_{-m'-m''}^{(-F'F'')}|$ . Obviously, that this relationship will not be changed by the atom-atom interaction (between work atoms), including the spin-exchange process. Therefore, the corresponding collisional frequency shifts have the same magnitude, i.e. they do not affect the frequency difference  $\Delta_{\pm}$  (while the collisional *broadening* of the EIT-resonances will have an influence). This property gives a significant advantage in comparison to other schemes of atomic magnetometers, where the atom-atom interaction is a limiting factor of the precision magnetic field measurement. The property (III) also support a certain optimism on the using of the miniature size cells in the EIT differential magnetometer, because it is possible to work at high cell temperature to get high atomic density (to significantly increase the signal/noise ratio).

Note, the property (III) can be extended to an arbitrary element (i.e. not only  $^{87}\text{Rb}$ ) and a resonance line,

when magnetometer uses the frequency difference between two-photon resonances  $m \leftrightarrow m$  and  $(-m) \leftrightarrow (-m)$ . In general, the angle  $\theta$  (between vectors  $\mathbf{B}$  and  $\mathbf{e}$ ) can be arbitrary as well.

The property (IV) is followed from two circumstances. Firstly, because the dark states nullify the resonant interaction (1) the light shifts of two-photon resonances (see Fig. 2, red solid line) via upper level  $F_e=1$  are absent. Therefore, the light shifts of  $\Delta_{\pm}$  are small and occur mostly from the interaction with far-off-resonance level  $F_e=2$ , see Fig. 1. Secondly, due to a symmetry these shifts are practically identical and compensate each other. Small disbalance exists and is caused by Zeeman splitting ( $\Delta_Z$ ). This splitting leads to the small difference for all one-photon detunings near dark resonances  $(+1) \leftrightarrow (+1)$  and  $(-1) \leftrightarrow (-1)$ . If the value of the light shift for each extreme resonances is  $U$ , then the relative shift can be estimated as  $\sim |\Delta_Z/\delta_{hfs}||U|$ , i.e. here we see a significant suppression of shifts by the factor  $|\Delta_Z/\delta_{hfs}| \ll 1$ .

In our case the magnetometer sensitivity  $\delta B$  depends on the signal-to-noise ratio (S/N) of the Zeeman resonance signal and the width of the EIT resonance  $\Gamma_{\text{FWHM}}$ :  $\delta B = \Delta B/(S/N)$ , where  $\Delta B = \Gamma_{\text{FWHM}}/\gamma'$  (see above the gyromagnetic ratio  $\gamma'$ ). Therefore, a high contrast of the  $\Lambda$ -resonances, where most of atoms ((50-70)%) are accumulated [19–21], makes them a perspective challenger for the existing all-optical magnetometers [17]. As an example, let's estimate the achievable sensitivity referencing to the recently published data on the lin||lin resonances [23] (authors of [23] characterized the lin||lin resonances in view of the perspective atomic clock reference). At resonance width  $\Gamma_{\text{FWHM}}=900$  Hz and  $S/N = 3.3 \times 10^3$  Hz<sup>1/2</sup> the sensitivity on the magnetic field is  $\delta B < 10^{-11}$  T/Hz<sup>1/2</sup>, which can be obtained without special efforts and for very moderate density  $10^{10}$  cm<sup>-3</sup> of rubidium atoms (50 C° and 1.2 Torr  $N_2$  pressure in [23]). To improve a sensitivity one should increase the number of atoms and narrow the resonance width. In this case the EIT differential magnetometer will achieve the sensitivity at the level  $\delta B \sim 10^{-13}$ - $10^{-14}$  T/Hz<sup>1/2</sup> or better, because we expect to reach the atom concentration more than  $10^{12}$  cm<sup>-3</sup> and meet no the limitation caused by the collisional process (see the property (III)). The proper option of the buffer gas pressure and the additional narrowing of the EIT resonance in dense media [26, 27] gives some advantages too. However, it's worth noting that the behavior of the coherent effects (EIT) in dense vapor  $>10^{12}$  cm<sup>-3</sup> is not studied yet in details, though, it is known that at  $10^{14}$  cm<sup>-3</sup> the EIT is still manifested [28].

Additionally here we should note that the each of  $\Lambda_3$  and  $\Lambda_4$  resonances (i.e.  $(-1) \leftrightarrow (-1)$  and  $(+1) \leftrightarrow (+1)$  two-photon transitions) also can be used in compass regime (described in the previous section III). But in this case there are few drawbacks compare to the compass based on the central resonance (i.e.  $\Lambda_{1,2}$ ). First, the frequency position of each of the resonances depends on the mag-

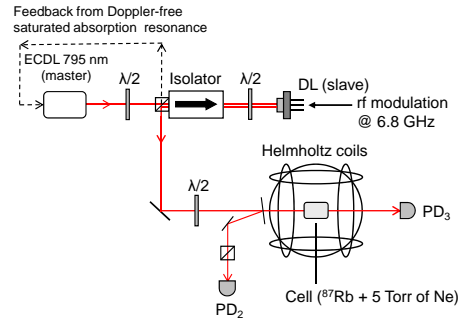


FIG. 4: The schematic of the experimental setup.

netic field. Second, their transmission dependence vs rotation of the vector  $\mathbf{e}(\varphi)$  can have two local maximum. One of them (which always exists) corresponds to the case  $\mathbf{e} \perp \mathbf{B}$ , but the other possible maximum emerges, when the vector  $\mathbf{e}$  lies in the plane  $(\mathbf{k}, \mathbf{B})$ . Such situation leads to an uncertainty in the measurement procedure.

## V. EXPERIMENT

From our point of view the possibility of the EIT-based compass is most attractive and unusual part of suggested ideas. Therefore, in experimental part we concentrate on the idea of EIT-based compass. The experimental setup is shown in Fig. 4. The bichromatic field  $\mathbf{E}(\mathbf{r}, t)$  is delivered by a grating laser diode EC DL, which frequency is modulated at  $\Delta_{hfs}=6.8$  GHz and injected into the slave laser diode DL [20]. The experiment is carried out on a Pyrex cell (40 mm long and 25 mm in diameter) containing isotopically enriched  $^{87}\text{Rb}$  and 4 Torr neon buffer gas. The cell is placed inside Helmholtz coils, where the field inhomogeneity is  $\sim 2$  mG/cm. For the experiments reported here the cell temperature is 45° C.

Laser frequency is locked to Doppler-free saturated absorption resonance. The radiation power at the cell front windows equals 1.5 mW. To excite the  $\Lambda_{1,2}$  transitions the light carrier is tuned at  $F_2 = 2 \rightarrow F_e = 1$  and the high frequency side-band is tuned at  $F_1 = 1 \rightarrow F_e = 1$  transitions. The registered spectra of the EIT resonances are shown in Fig. 2, where the curves correspond to the  $^{87}\text{Rb}$  transmission spectra for two cases:  $\mathbf{e} \parallel \mathbf{n}$  and  $\mathbf{e} \perp \mathbf{n}$ .

Before entering the cell light propagates through a half-wave plate, which is rotated at 13 Hz rate. In result, we detect the light transmission on the angle between  $\mathbf{e}$  and  $\mathbf{B}$ , see Fig. 5. It's worth noting that the light transmission is affected by the changes of the EIT transmission and the optical pumping. The  $\pi$ -polarization component (at  $(\varphi \neq \pi/2)$ ) of the excitation beam causes a pump of a large portion of the atoms into the trap states of  $m_F = \pm 2$  Zeeman sublevels. This effectively reduces the number of interacting atoms resulting in the increasing of the overall transmission. To avoid this distortion of the transmission we detect signals at the second harmonic of the rf-modulated polarization which is done by Faraday



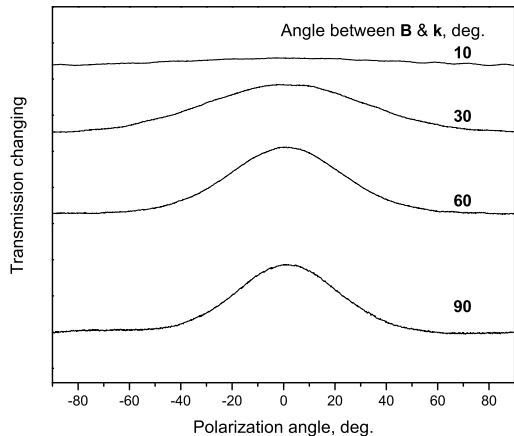


FIG. 5: Changing of the EIT-resonance amplitude  $A(\varphi)$  for the  $^{87}\text{Rb}$  cell transmission on the angle  $\varphi$  between  $\mathbf{e}$  and  $\mathbf{n}$ . An angle between  $\mathbf{B}$  and  $\mathbf{k}$  are shown on the right side of each curve (both vectors lie in the horizontal plane).

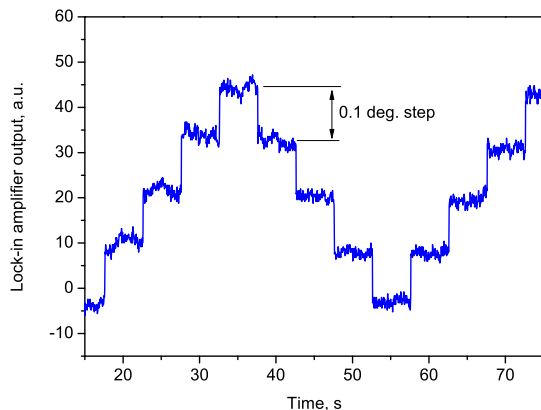


FIG. 6: The lock-in amplifier output at  $0.1^\circ$  angle step variation of the magnetic field direction. The magnetic field magnitude is 1 G, the angle between magnetic field and wave vector is  $90^\circ$ .

modulator at 7.6 kHz.

To determine the detection sensitivity of the vector's  $\mathbf{B}$  direction we change the orientation of the magnetic field by  $0.1^\circ$  steps. The lock-in amplifier output denotes these steps, from which we estimate a sensitivity, that is  $\sim 10^{-3} \text{ deg/Hz}^{1/2}$ , see Fig. 6. This data was taken for  $\varphi = 90^\circ$  at 1 G magnetic field, the detection bandwidth is 300 Hz.

We discovered that the sensitivity depends on the magnitude of the applied magnetic field (see Fig. 7). At low magnetic field the sensitivity degrades almost two order

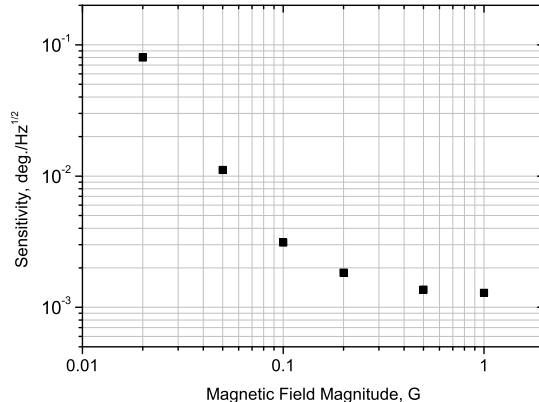


FIG. 7: Compass sensitivity vs. magnetic field magnitude.

compare to those of 0.1-7 G. In the absence of a magnetic fields the overall light transmission is exposed, but this coincides with a low EIT-resonance contrast. This occurs due to trap states belonging to the degenerate Zeeman sublevels of the same hyperfine level where atoms “hide”. The contrast (as well as signal/noise ratio) grows upon the appearance of the magnetic field. This caused by the removal of the sublevel degeneration. To destroy trap states, a magnetic field should possess the magnitude at which the splitting between the (0-0) (i.e.  $\Lambda_{1,2}$ ) and (1-1) (i.e.  $\Lambda_{3,4}$ ) transitions is equal to the resonance width. Once the (0-0) and (1-1) transitions are separated at  $\sim 0.1$  G (in our setup) the compass has the best sensitivity for  $|\mathbf{B}| > 1$  G. Note, for some magnetic field ( $|\mathbf{B}| > 5$  G in our experiments) the central resonance begins to split [19–21, 29], because the  $\Lambda_1$  and  $\Lambda_2$  transitions have a small difference in  $g$ -factors (2.8 kHz/G) due to nuclear spin. However, this effect itself does not set the upper operational limit of the magnetic field for the vector measurements (compass), because in this case we can work with one of two separated  $\Lambda$ -resonances. We believe that the upper limitation on magnetic field in our method is connected with degradation of EIT-resonances, when the value  $\mu_B B$  is comparable with excited state hyperfine splitting  $\delta_{hfs} \approx 812$  MHz, i.e. due to a strong magnetic mixing between upper hyper-fine levels  $F_e=1$  and  $F_e=2$  (see Fig. 1). Summing what is discussed above, for parameters of our setup the magnetic field operational range of the 3D compass is about  $\sim 0.1$ -200 G.

## VI. CONCLUSION

In conclusion, we develop the generalized principle of the atomic vector magnetometry based on high-contrast EIT-resonances in linear polarized field. It is shown that this principle is valid for any atoms. The compass with using of two non-parallel laser beams allows to measure

the orientation of the magnetic field in three dimensions. We have achieved in our proof-of-principle experiment a compass sensitivity  $\sim 10^{-3}$  deg/Hz $^{1/2}$  at intermediate magnetic fields. We have found that major contribution to the sensitivity gives the noise level mostly related to the intensity fluctuation of the laser system. Thus, we believe that the proposed method has a potential to achieve the angle sensitivity at the level  $\sim 10^{-4}$  deg/Hz $^{1/2}$ .

Also we discuss the advantages of the suggested magnetometer such as the non-sensitivity to the quadratic Zeeman and ac-Stark effects, atom-buffer gas and the atom-atom collisions. Moreover, our EIT magnetometer will work for arbitrary mutual orientation between wavevector  $\mathbf{k}$  and magnetic vector  $\mathbf{B}$ . A proper choice of the buffer gas type, pressure, the cell with the anti-relaxation coating walls [11], and the cell volume enable the varying of sensitivity, the spatial resolution, and the

working range of the magnetic field.

The EIT vector magnetometer can be important for non-invasive biomedical studies [30, 31] of the temporal and spacial distribution of the brain and heart currents. Recent successes in the developing the chip-size atomic clock and magnetometer [32] give the legitimate optimism on the creation of the small size sensor. At whole, the proposed compass-magnetometer could find a broad variety of application in physics, navigation, geology, biology, medicine, industry and so on.

We thank L. Hollberg, H. Robinson, J. Kitching, F. Levi, S. Knappe, V. Shah, V. Gerginov and P. Schwindt for helpful discussions. V.I.Yu. and A.V.T. were supported by RFBR (08-02-01108, 10-02-00591, 10-08-00844) and programs of RAS.

V. I. Yudin e-mail address: viyudin@mail.ru

S. A. Zibrov e-mail address: serezhza.zibrov@gmail.com

- 
- [1] G. Alzetta, A. Gozzini, L. Moi, and G. Orriols, *Il Nuovo Cim.* **36B**, 5 (1976).
  - [2] E. Arimondo, in *Progress in Optics*, ed. by Wolf E., Vol. **XXXV**, 257 (1996).
  - [3] S. E. Harris, *Physics Today* **50**(7), 36 (1997).
  - [4] M. Fleischhauer, M. A. Imamoglu, and J. P. Marangos, *Rev. Mod. Phys.* **77**, 633 (2005).
  - [5] M. Fleischhauer and M. O. Scully, *Phys. Rev. A* **49**, 1973 (1994).
  - [6] S. Pustelny, J. Kimball, S. M. Rochester, V. V. Yashchuk, W. Gawlik, and D. Budker, *Phys. Rev. A* **73**, 23817 (2006).
  - [7] I. Novikova, A. B. Matsko, V. L. Velichansky, and G. R. Welch, *Phys. Rev. A* **56**, R1063 (2001).
  - [8] M. Stähler, S. Knappe, C. Affolderbach, W. Kemp and R. Wynands, *Europhys. Lett.* **54**, 323 (2001).
  - [9] C. Affolderbach, M. Stähler, S. Knappe, and R. Wynands, *Appl. Phys. B* **75**, 605 (2002).
  - [10] V. Acosta, M. P. Ledbetter, S. M. Rochester, D. Budker, D. F. J. Kimball, D. C. Hovde, W. Gawlik, S. Pustelny, J. Zachorowski, and V. V. Yashchuk, *Phys. Rev. A* **73**, 053404 (2006).
  - [11] D. Budker and M. Romalis, *Nature Physics*, **3**, 227 (2007).
  - [12] I. K. Komonis, T. W. Kornack, J. C. Allred, and M. V. Romalis, *Nature (London)* **422**, 596 (2003).
  - [13] A. J. Fairweather and M. J. Usher, *J. Phys. E* **5**, 986 (1972).
  - [14] E. B. Alexandrov, M. V. Balabas, V. N. Kulyasov, A. E. Ivanov, A. S. Pazgalev, J. L. Rasson, A. K. Vershovskii, and N. N. Yakobson, *Meas. Sci. Technol.* **15**, 918 (2004).
  - [15] O. Gravrand, A. Khokhlov, J. L. Le Mouél, and J. M. Léger, *Earth Planets Space* **53**, 949-958, (2001).
  - [16] D. Budker and M. Romalis, *Nature Physics* **3**, 227 (2007).
  - [17] E. B. Alexandrov and A. K. Vershovskii, *Phys. Usp.* **52**, 573 (2009).
  - [18] A. V. Taichenachev, V. I. Yudin, V. L. Velichansky, A. S. Zibrov, and S. A. Zibrov, *Phys. Rev. A* **73**, 013812 (2006).
  - [19] S. A. Zibrov, Y. O. Dudin, V. L. Velichansky, A. V. Taichenachev, V. I. Yudin, Abstract Book and Technical Digest of ICONO'05 (St. Petersburg, Russia, 11-15 May 2005), ISK8 (2005).
  - [20] A. V. Taichenachev, V. I. Yudin, V. L. Velichansky, and S. A. Zibrov, *JETP Lett.* **82**, 449 (2005).
  - [21] S. A. Zibrov, V. L. Velichansky, A. S. Zibrov, A. V. Taichenachev, and V. I. Yudin, *JETP Lett.* **82**, 477 (2005).
  - [22] S. A. Zibrov, I. Novikova, D. F. Phillips, R. L. Walsworth, A. S. Zibrov, V. L. Velichansky, A. V. Taichenachev, and V. I. Yudin, *Phys. Rev. A* **81**, 013833 (2010).
  - [23] E. Breschi, G. Kazakov, R. Lammegger, B. Matisov, L. Windholz, and G. Miletì, *IEEE Transactions on Ultrasonics, Ferroelectrics, and Frequency Control* **56**, 926 (2009).
  - [24] E. Arimondo, M. Inguscio, and P. Violino, *Rev. Mod. Phys.* **49**, 31 (1977).
  - [25] D. A. Steck, "Rubidium 87 D Line Data", available online at <http://steck.us/alkalidata> (revision 2.0.1, 2 May 2008).
  - [26] M. D. Lukin, M. Fleischhauer, A. S. Zibrov, H. G. Robinson, V. L. Velichansky, L. Hollberg, and M. O. Scully, *Phys. Rev. Lett.* **79**, 2959 (1997).
  - [27] E. E. Mikhailov, V. A. Sautenkov, Yu. V. Rostovtsev, A. Zhang, M. S. Zubairy, M. O. Scully, and G. R. Welch, *Phys. Rev. A* **74**, 013807 (2006).
  - [28] A. S. Zibrov, A. B. Matsko, L. Hollberg, and V. L. Velichansky, *J. Mod. Opt.* **49**, 359 (2002).
  - [29] G. Kazakov, B. Matisov, I. Mazets, G. Miletì, and J. Delporte, *Phys. Rev. A* **72**, 063408 (2005).
  - [30] G. Bison, R. Wynands, and A. Weis, *Appl. Phys. B* **76**, 325 (2003).
  - [31] G. Bison, R. Wynands, and A. Weis, *Opt. Expr.* **11**, 904 (2003).
  - [32] P. Schwindt, S. Knappe, V. Shah, L. Hollberg, J. Kitching, L. Liew, and L. Moreland, *Appl. Phys. Lett.* **85**, 6409 (2004).